International Journal of Engineering Research & Technology (IJERT)
ISSN: 2278-0181
Vol. 15 Issue 08 , August - 2026

Prediction of Polyhouse Roof Truss Members using MLP and MNM

Deepak Kulyal[1], V. K. Verma[2], Karan Sati[3]

[1] Research Scholar, Department of Civil Engineering, College of Technology, G.B.P.U.A.T., Pantnagar, UK, India.
[2] Associate Professor, Department of Civil Engineering, College of Technology, G.B.P.U.A.T., Pantnagar, UK, India.
[3] Research Scholar, Department of Electrical Engineering, College of Technology, G.B.P.U.A.T., Pantnagar, UK, India.

Abstract: Polyhouses are specialised agricultural structures developed to maintain controlled environmental conditions for crop cultivation, thereby ensuring consistent productivity even under adverse climatic circumstances. The performance of these systems largely relies on the structural stability and cost efficiency of the roof truss, which must achieve an effective balance between strength, adaptability and economy. Designing that truss with finite element software is reliable but slow: every change of span, purlin spacing or load intensity requires a fresh analysis and design cycle.

This study develops and compares two artificial neural network surrogates for that cycle a Multilayer Perceptron (MLP), whose neurons aggregate their weighted inputs additively, and a Multiplicative Neuron Model (MNM), whose neurons aggregate them as a product. A dataset of 384 Howe-type polyhouse truss configurations, spanning a wide range of geometric parameters, purlin spacings and load combinations, was generated in STAAD.Pro and used to train both networks on identical data with an identical Levenberg–Marquardt procedure, so that any difference in accuracy is attributable to the neuron model rather than to the training algorithm. Eight input variables length, width, spacing between purlins, length of top chord, spacing of purlins, dead load, live load and wind load were mapped onto the six optimised member cross-sectional areas of the riser, rafter, vertical chord, inclined chord, purlins and column.

With a conventional random 70/15/15 partition, the MLP reproduced the STAAD.Pro areas with an overall RMSE of 0.286 cm² ($R = 0.9957$, $R^2 = 0.9914$) and the MNM with 0.331 cm² ($R = 0.9942$, $R^2 = 0.9885$). Because the dataset is composed of 64 distinct design cases repeated at six polyhouse lengths, both networks were additionally retrained with whole design cases withheld; testing RMSE then rose to 0.402 cm² for the MLP and 0.453 cm² for the MNM, which is the figure that reflects prediction for an unseen geometry. The MLP was more accurate overall, driven by the rafter, while the MNM predicted the vertical chord, inclined chord and column more accurately, consistent with its ability to represent products of span and load directly. Both models size a truss in a fraction of a second against a full analysis-and-design cycle, and the proposed framework therefore offers a rapid, reliable route to preliminary design, parametric study and structural optimisation of protected agricultural infrastructure.

Keywords Artificial Neural Network (ANN), Multilayer Perceptron (MLP), Multiplicative Neuron Model (MNM), STAAD.Pro, Polyhouse, Truss, Surrogate model.

INTRODUCTION

Polyhouse structures have become an integral component of modern protected agriculture by providing a controlled environment that regulates temperature, humidity, ventilation and solar radiation, thereby enabling year-round crop production. Unlike conventional open-field cultivation, polyhouses protect crops from adverse environmental conditions while improving productivity and resource utilisation. The structural performance of a polyhouse primarily depends on its roof truss system, which must safely resist dead, live and wind loads while maintaining adequate strength, stiffness, durability and economy. Owing to their high strength-to-weight ratio, corrosion resistance and ease of fabrication, Circular Hollow Sections (CHS) are widely adopted for polyhouse roof trusses.

The structural design of polyhouse roof trusses is generally performed using finite element analysis (FEA)-based software such as STAAD.Pro, which accurately evaluates member forces, deformations and code compliance under multiple loading combinations. Although this approach produces reliable designs, it becomes computationally intensive and time-consuming when a large number of geometric configurations and loading scenarios are analysed. Consequently, repeated structural analyses and iterative member selection reduce design efficiency and limit the rapid development of economical polyhouse structures.

Recent advances in machine learning have provided an effective alternative for modelling the complex nonlinear relationships encountered in structural engineering. Among these techniques, the Multilayer Perceptron (MLP) has demonstrated excellent capability in approximating highly nonlinear structural responses through feedforward learning. Its neurons, however, aggregate their weighted inputs by summation, so an interaction between two design variables the product of span and load intensity, for instance can only be approximated indirectly, by combining several additive units. The Multiplicative Neuron Model (MNM), introduced by Yadav et al. (2007), replaces the summation inside the neuron with a product, which allows a single unit to represent such interactions directly and often yields comparable accuracy from a more compact network.

Despite the growing application of machine learning in structural engineering, comparative studies investigating the performance of MLP and MNM for predicting optimum member sections of polyhouse roof trusses remain limited. To address this research gap, the present study develops a comparative machine learning framework for predicting the

International Journal of Engineering Research & Technology (IJERT)
ISSN: 2278-0181
Vol. 15 Issue 08 , August - 2026

cross-sectional areas of steel pipe members in Howe-type polyhouse roof trusses. A dataset comprising 384 STAAD.Pro-generated truss models under varying geometric configurations and environmental loading conditions was used to train and evaluate both models. Their predictive performance was assessed on identical data using identical statistical measures, and because the dataset contains repeated design cases under two distinct partitioning schemes, so that memorisation and genuine generalisation could be separated. The proposed framework aims to minimise dependence on repeated finite element analyses while providing accurate, reliable and economical predictions of truss member cross-sectional areas, thereby supporting intelligent structural design and automation in protected agricultural infrastructure.

LITERATURE REVIEW

The structural design of polyhouses and greenhouse systems has been widely investigated with emphasis on structural optimisation, material efficiency and resistance to environmental loading. Early research by Amir and Hasegawa (1988) introduced discrete optimisation techniques based on the Modified Rosenbrock Orthogonalisation Procedure and gradient-based algorithms for greenhouse structural design. Their study demonstrated that appropriate selection of steel member sections significantly enhances structural performance while reducing material consumption and overall construction cost, highlighting the importance of optimisation in lightweight greenhouse frameworks.

Subsequent studies shifted the focus towards computational structural analysis. Mandalik (2001) and Çağdaş (2004) demonstrated the effectiveness of finite element analysis using commercial software such as SAP2000 for evaluating the static and dynamic behaviour of truss systems, establishing that computational modelling provides a reliable means of assessing structural response under various loading conditions and thereby improving the safety, durability and material efficiency of greenhouse structures. Collectively, these studies established FEA as an indispensable tool for analysing complex structural behaviour and supporting the design of economical and reliable polyhouse systems.

Region-specific studies have highlighted the influence of structural configuration, geometry and load distribution on greenhouse performance under environmental loads. Kendirli (2006) emphasised the importance of detailed structural analysis to ensure adequate resistance against wind and snow loads. Kalyanshetti and Mirajkar (2012) demonstrated that tubular steel sections provide superior strength-to-weight ratio, structural efficiency and economy, making them well suited for lightweight agricultural structures. Choi et al. (2014) documented greenhouse construction practices in Korea, contributing to the development of standardised design guidelines and improved structural safety.

Wind loading is recognised as a primary governing factor in the design and stability of greenhouses. Improper assessment of wind-induced pressures and load paths can lead to severe structural failures and significant economic losses, underscoring the necessity of accurate load determination using established standards such as IS 875 (Part 3), particularly in high-wind regions (Nayak et al., 2018; Saltuk, 2019). Evaluating complex load interactions across various greenhouse types further reveals that structural components often require specific modifications to safely withstand combined environmental loading scenarios (Singh et al., 2021).

Parallel to advances in traditional structural analysis, Artificial Neural Networks (ANNs) have emerged as powerful computational tools in civil engineering. Early research demonstrated their ability to recognise complex behaviours, such as diagnosing damage in truss joints using limited measurement data (Mehrjoo et al., 2008; Dai and Wang, 2007). ANNs were soon established as efficient surrogates for conventional software, with studies achieving prediction errors as low as 2.51 % in the fully stressed design of trusses (Saxena and Pathak, 2015). Building on this computational efficiency, Erdal and Karakuzu (2018) developed an MLP model trained on finite element data to accurately predict the nonlinear responses of steel frames, proving that ANN-based surrogate models drastically reduce computational time for preliminary designs a methodology readily translatable to truss structures. More recently, machine learning applications have expanded further, leveraging Convolutional Neural Networks to achieve high predictive accuracy for structural health monitoring in large-span truss systems (Liu et al., 2021; Gao and Yang, 2021).

The multiplicative neuron formulation adopted here originates outside structural engineering. Yadav et al. (2007) proposed a single neuron whose aggregation function is a product of affine terms, and showed that it matched or exceeded conventional multilayer networks on nonlinear time-series problems while using far fewer parameters. The formulation has since been applied to forecasting and function approximation, but comparative evaluations against conventional MLPs on structural design data are scarce.

The literature therefore reveals two converging trends: the increasing adoption of FEA-based computational tools for accurate polyhouse structural design, and the growing application of machine learning techniques for structural prediction and optimisation. Studies employing advanced neural network architectures particularly a direct comparison of MLP and MNM for predicting optimal member sections of polyhouse roof trusses using large, systematically generated computational datasets remain scarce. The present study integrates STAAD.Pro-generated data with both architectures to develop a rapid, accurate and computationally efficient framework for predicting and optimising steel pipe sections in polyhouse roof trusses.

MATERIALS AND METHODS

1. Steel Pipe Sections (Circular Hollow Sections)

Circular Hollow Sections (CHS) were selected for the polyhouse roof truss owing to their high strength, excellent buckling resistance, uniform load transfer and favourable strength-to-weight ratio. Their geometric symmetry, corrosion resistance and ease of fabrication make them particularly suitable for lightweight agricultural structures. All sections conform to IS 1161:2014, ensuring uniform mechanical and dimensional properties. The section database includes light, medium and heavy class steel pipes with diameters ranging from 21.3 mm to 355.6 mm and corresponding cross-sectional areas between 1.21 cm² and

International Journal of Engineering Research & Technology (IJERT)
ISSN: 2278-0181
Vol. 15 Issue 08 , August - 2026

87.4 cm². These cross-sectional areas constitute the target output variables for training the MLP and MNM to predict appropriate member sizes under varying geometric and loading conditions.

2. Structural Modelling via STAAD.Pro

A systematic computational workflow was established to generate the dataset required to train the predictive models. Using STAAD.Pro, structural analyses and designs of Howe-type roof trusses were conducted across a wide spectrum of geometric configurations and environmental loading conditions. The principal steps are outlined below and summarised in Fig. 6.

(a) Geometry definition. Using the STAAD.Pro Structure Wizard, a standard Howe truss template was adapted to construct polyhouse frameworks. A diverse dataset was generated by altering core geometric parameters overall length (10–50 m), width or span (5–20 m), spacing between purlins (2–5 m), top chord length (4.10–10.51 m) and panel point distribution. These systematic modifications produced 384 structurally distinct models, providing the foundation for the subsequent analysis.

(b) Load calculations. Load intensities were derived in compliance with the relevant Indian Standard codes. Dead loads, encompassing the self-weight of the truss members, purlins and polycarbonate roofing, were evaluated as per IS 875 (Part 1). Live loads were calculated according to IS 875 (Part 2), with adjustments for roof slope and cross-verification against the IS 14462:1997 guidelines for greenhouses. Wind loads were computed using IS 875 (Part 3), factoring in terrain, topography, risk coefficients and hill-region effects to determine the design wind speed and the corresponding internal and external pressure coefficients. A regional design wind speed of 37 m/s was adopted, as mandated by the IS codes for the Almora district of Uttarakhand, India. Across the dataset the resulting intensities span 0.62–6.20 kN/m² (dead), 0.80–7.70 kN/m² (live) and 2.98–19.10 kN/m² (wind).

(c) Assignment of section properties and boundary conditions. Circular hollow pipe sections were assigned to all primary truss components risers, rafters, vertical chords, inclined chords, purlins and columns. Following the assignment of preliminary trial sections based on engineering judgement, the STAAD.Pro design module (in compliance with IS 800:2007) performed iterative optimisation, refining the member sizes until all elements satisfied the required strength and serviceability criteria. This iterative design cycle generated the optimised cross-sectional areas for each configuration, which subsequently served as the target output dataset for training the predictive models. Table 1 lists a representative set of sections returned by this procedure.

Table 1: Compatible sections of the roof truss that pass the design calculation

Sr. No.	Members	Reaction	Section	Area of cross-section (cm²)
1	Riser	R1	603H	5.23
2	Rafter	R2	269L	1.78
3	Vertical chord	R3	424H	4.83
4	Inclined chord	R4	424L	4.83
5	Purlins	R5	213L	1.21
6	Column (eave level)	R6	889L	8.62

(d) Repeated modelling for dataset generation. The complete design procedure was repeated for 384 polyhouse configurations, each representing a unique combination of truss length, span, top chord length, purlin spacing, panel points and dead, live and wind loads. This produced a supervised dataset of eight input variables and six output variables corresponding to the riser, rafter, vertical chord, inclined chord, purlins and column. For each configuration the optimum cross-sectional area and the corresponding standard pipe section of every truss component were recorded. Table 2 summarises the range of every variable.

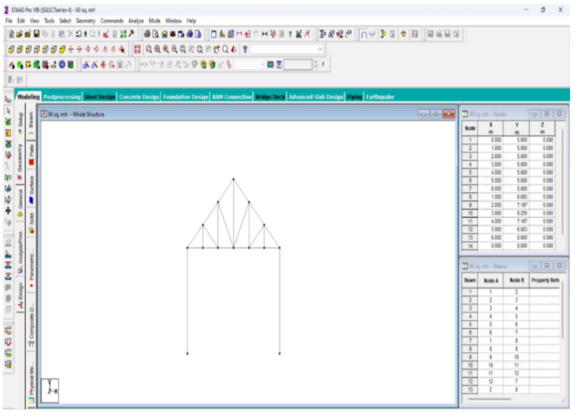

Fig. 1: Geometric modelling of the polyhouse frame in STAAD.Pro

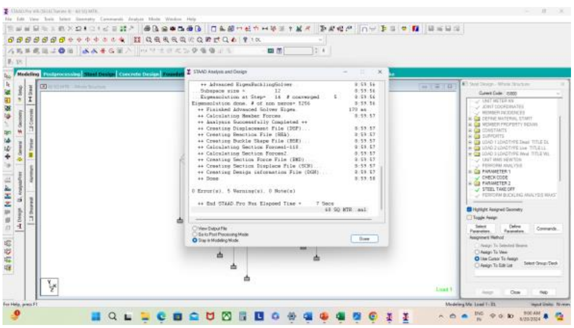

Fig. 2: Structural analysis and steel design run in STAAD.Pro

Table 2: Input and output variables of the dataset (384 configurations)

Role	Variable	Unit	Minimum	Maximum	Distinct values
Input	Polyhouse length	m	10.00	50.00	19
Input	Width / span	m	5.00	20.00	16
Input	Spacing between purlins	m	2.00	5.00	4
Input	Length of top chord	m	4.10	10.51	16

International Journal of Engineering Research & Technology (IJERT)
ISSN: 2278-0181
Vol. 15 Issue 08 , August - 2026

Role	Variable	Unit	Minimum	Maximum	Distinct values
Input	Spacing of purlins	m	1.37	3.50	16
Input	Dead load (DL)	kN/m^2	0.62	6.20	64
Input	Live load (LL)	kN/m^2	0.80	7.70	43
Input	Wind load (WL)	kN/m^2	2.98	19.10	62
Output	Riser area	cm^2	5.23	7.89	3
Output	Rafter area	cm^2	1.78	18.50	18
Output	Vertical chord area	cm^2	3.25	4.83	3
Output	Inclined chord area	cm^2	4.14	7.33	4
Output	Purlins area	cm^2	1.21	3.25	4
Output	Column area	cm^2	8.62	12.50	3

ARTIFICIAL NEURAL NETWORK MODELLING

3.1 Structure of the dataset

Before any model was fitted, the dataset was examined for repeated design cases. The 384 records reduce to 64 distinct combinations of width and spacing between purlins, each repeated at six different polyhouse lengths. Within any one of these design cases none of the six member areas changes, and the remaining inputs top chord length, spacing of purlins, dead load, live load and wind load are themselves fixed functions of width and purlin spacing. Polyhouse length therefore has no influence on the predicted member sizes anywhere in this dataset, and the effective input dimensionality is two rather than eight (Fig. 3).

This has a direct consequence for how accuracy must be reported. Under a random record-wise 70/15/15 partition, every testing record has five twins with identical targets sitting in the training set, so the testing error measures recall of a case the network has already seen. Both models were therefore evaluated twice: once under the conventional record-wise partition, to remain comparable with the ANN literature, and once with entire design cases withheld, to measure prediction for a polyhouse geometry the network has genuinely never encountered. Both sets of results are reported in the sections that follow.

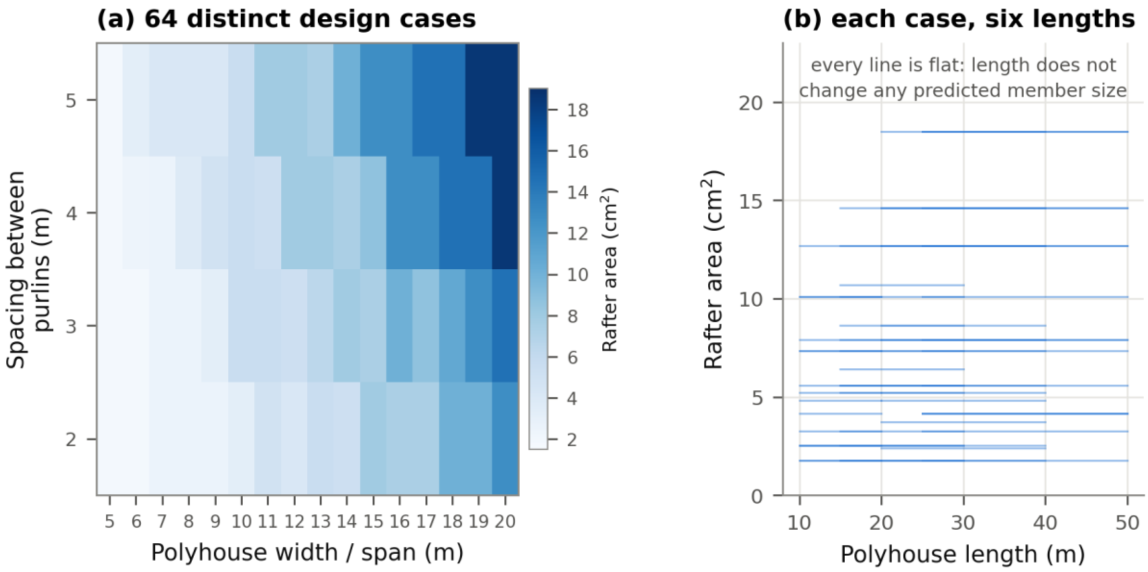

Fig. 3: Structure of the supplied dataset. (a) The 384 records form a 16 × 4 grid of 64 distinct design cases in width and purlin spacing. (b) Rafter area plotted against polyhouse length for every design case; each line is horizontal, confirming that length does not alter any predicted member size.

3.2 Network architectures

Both models share the same three-layer topology (Fig. 4a): an input layer of eight neurons corresponding to the structural variables, a single hidden layer of ten neurons, and an output layer of six neurons returning the target cross-sectional areas. The hidden layer uses the hyperbolic tangent sigmoid (tansig) transfer function and the output layer is linear (purelin). The two models differ only in the operation performed inside the hidden neuron (Fig. 4b).

In the MLP, the hidden neuron aggregates its weighted inputs additively:

$$net_h = \Sigma_i \, w_{hi} \, x_i + b_h \,, \qquad a_h = \mathrm{tansig}(net_h) \qquad \ldots(1)$$

In the MNM, the summation is replaced by a product over the eight affine terms, following Yadav et al. (2007):

$$net_h = \Pi_i \, (\, w_{hi} \, x_i + b_{hi} \,) \,, \qquad a_h = \mathrm{tansig}(net_h) \qquad \ldots(2)$$

In both cases the output layer combines the hidden activations linearly, y = V a + c. The product form allows a single multiplicative neuron to represent an interaction such

International Journal of Engineering Research & Technology (IJERT)
ISSN: 2278-0181
Vol. 15 Issue 08 , August - 2026

as span × load directly, whereas an additive neuron can only approximate it by combining several units. For ten hidden neurons the MLP carries 156 free parameters and the MNM 226, the difference arising because the MNM assigns an individual bias to each input of each hidden neuron.

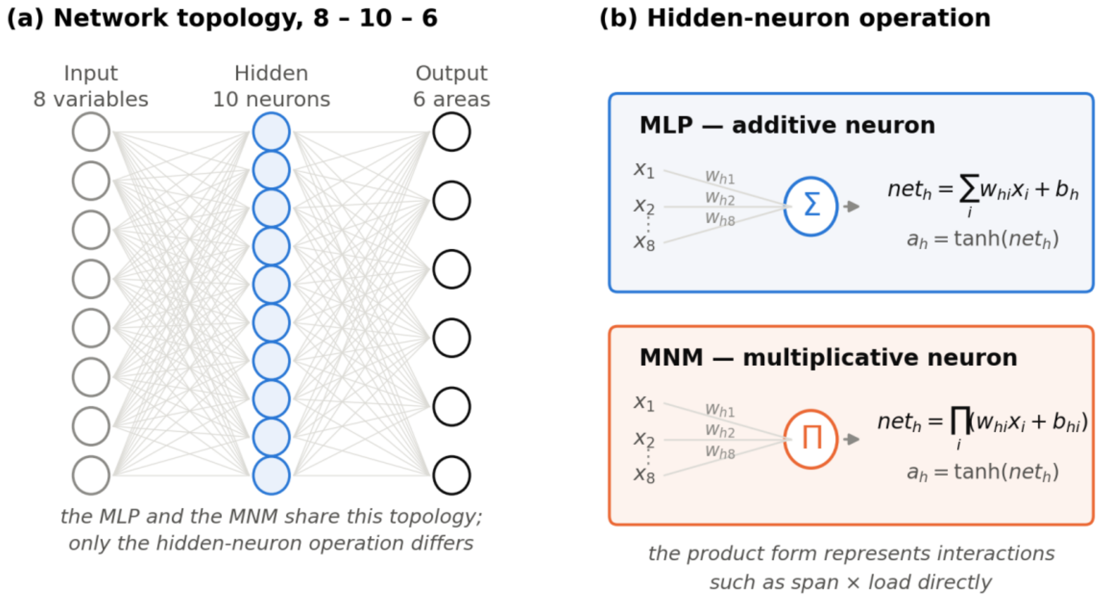

Fig. 4: Architecture of the two models. (a) Both networks share the 8 – 10 – 6 topology with tansig hidden and linear output layers. (b) The hidden neuron aggregates its weighted inputs by summation in the MLP and by multiplication in the MNM.

3.3 Training procedure

Both networks were trained by the Levenberg–Marquardt algorithm (trainlm), selected for its rapid convergence and suitability for medium-sized datasets, with analytically derived Jacobians. Applying the same optimiser, the same partition, the same scaling policy and the same stopping rules to both architectures ensures that any difference in predictive performance is attributable to the neuron model rather than to the training procedure. Inputs and targets were min–max scaled; for the MNM the inputs were scaled to [0.5, 1.5] rather than [−1, 1] so that the product of eight factors remains numerically well-conditioned, since a product of eight values drawn from [−1, 1] collapses towards zero and the gradients vanish with it.

Training ran for a maximum of 1000 epochs with mean squared error as the performance function and early stopping after six consecutive increases in validation error, the weights giving the best validation performance being retained. Five random restarts were performed for each configuration and the network with the lowest validation error was kept, which removes the dependence of the reported accuracy on a single fortunate or unfortunate initialisation. Table 3 summarises the training configuration.

Table 3: Training configuration common to both architectures

Training variable	Assigned value
Neural network	Feed-forward, back propagation
Hidden layers	1
Hidden neurons	10 (selected from a parametric evaluation of 1 to 20)
Transfer function	Tansig (hidden layer), Purelin (output layer)
Training function	TRAINLM (Levenberg–Marquardt)
Adaption learning function	LEARNGDM (gradient descent with momentum)
Performance function	MSE (mean squared error)
Maximum epochs	1000
Early stopping	6 consecutive validation failures
Random restarts	5, network with best validation error retained
Data division	70 % training / 15 % validation / 15 % testing
Input scaling	Min–max to [−1, 1] (MLP) and [0.5, 1.5] (MNM)
Target scaling	Min–max to [−1, 1]
Software	MATLAB R2021a; scripts also run in GNU Octave

3.4 Selection of the hidden-layer size

Networks with 1 to 20 hidden neurons were trained under identical conditions and compared on validation RMSE (Fig. 5, Table 4). Validation error falls steeply up to about six neurons for both architectures. Beyond that the MLP continues to improve and reaches a numerically exact fit at 18 to 20 neurons, whereas the MNM improves more

International Journal of Engineering Research & Technology (IJERT)
ISSN: 2278-0181
Vol. 15 Issue 08 , August - 2026

gradually and attains its best validation error at 18 neurons. Ten neurons the configuration adopted for the main comparison, and the value reported in the earlier version of this work is therefore a defensible compromise between accuracy and compactness rather than a minimum of the validation curve, and is treated as such throughout.

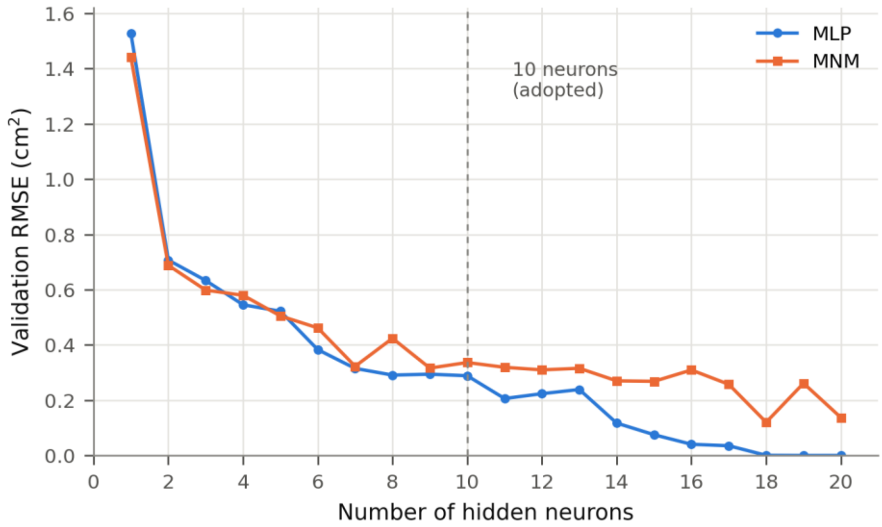

Fig. 5: Parametric evaluation of hidden-layer size. Validation RMSE for 1 to 20 hidden neurons under identical training conditions.

Table 4: Parametric evaluation of hidden-layer size (record-wise partition)

Hidden neurons	MLP validation RMSE (cm^2)	MLP testing RMSE (cm^2)	MNM validation RMSE (cm^2)	MNM testing RMSE (cm^2)
1	1.527	1.692	1.441	1.479
2	0.707	0.748	0.688	0.718
4	0.545	0.630	0.580	0.655
6	0.383	0.365	0.462	0.519
8	0.291	0.307	0.424	0.417
10	0.288	0.282	0.336	0.407
12	0.224	0.210	0.310	0.305
14	0.117	0.127	0.270	0.242
16	0.040	0.028	0.309	0.299
18	0.00047	0.00042	0.120	0.110
20	0.000017	0.000017	0.137	0.139

3.5 Performance metrics

The predictive performance of both models was evaluated using the root mean square error (RMSE), which measures the average magnitude of the deviation between the observed and predicted cross-sectional areas of the steel pipe members. A lower RMSE indicates higher prediction accuracy:

$$\mathrm{RMSE} = \sqrt{ (1/n) \Sigma_{i=1} [Q_{oi} - Q_{pi}]^2 } \qquad \ldots(3)$$

where Q_{oi} is the i-th observed value of the cross-sectional area of the steel pipes, Q_{pi} the i-th predicted value and n the number of observations.

The correlation coefficient is obtained from:

$$R = \Sigma (Q_{oi} - \bar{Q}_o) (Q_{pi} - \bar{Q}_p) \div \sqrt{ \Sigma (Q_{oi} - \bar{Q}_o)^2 \cdot \Sigma (Q_{pi} - \bar{Q}_p)^2 } \qquad \ldots(4)$$

where $\bar{Q}_o$ and $\bar{Q}_p$ denote the mean observed and mean predicted cross-sectional areas respectively. The coefficient of determination $R^2 = 1 - SSE/SST$, the mean absolute error (MAE) and the mean absolute percentage error (MAPE) were computed alongside these two measures.

A further, design-oriented measure is also reported. Because the STAAD.Pro design module returns a standard catalogue section rather than a continuous area, each prediction was rounded to the nearest area available for that member and compared with the section STAAD.Pro actually selected. The resulting standard-section hit rate expresses accuracy in the terms an engineer uses: the proportion of configurations for which the network specifies the correct pipe. A model may have a low RMSE and still choose the wrong section when two catalogue sizes lie close together, so the two measures are complementary.

International Journal of Engineering Research & Technology (IJERT)
ISSN: 2278-0181
Vol. 15 Issue 08 , August - 2026

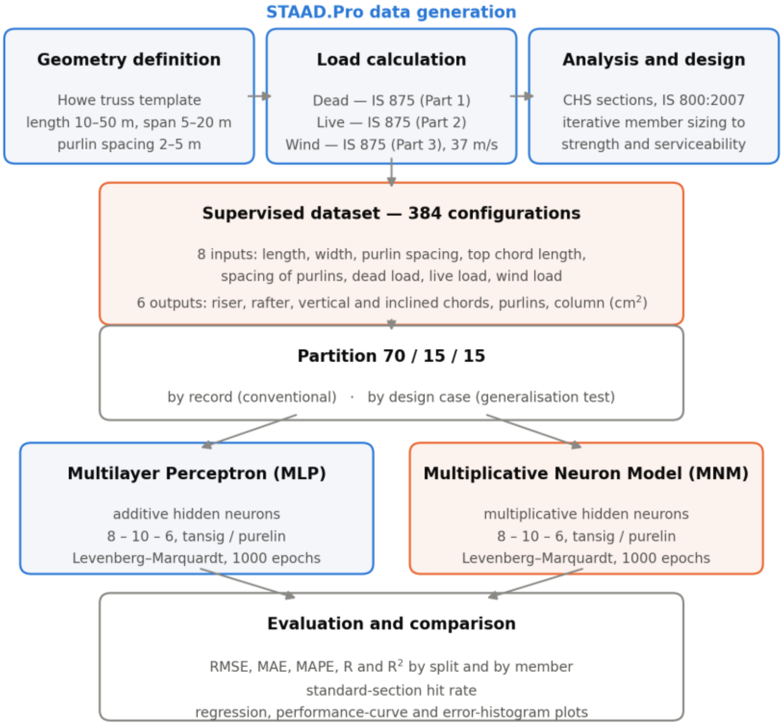

Fig. 6: Methodology for developing the MLP and MNM models using STAAD.Pro-generated data.

RESULTS AND DISCUSSION

4.1 Dataset generated by STAAD.Pro

Structural modelling in STAAD.Pro yielded a dataset of 384 distinct polyhouse truss configurations covering a wide range of geometric parameters and environmental loading conditions. For each configuration, structurally safe and economically optimised cross-sectional areas were determined for all primary members. The analysis evaluated diverse load combinations and incorporated a regional design wind speed of 37 m/s. These optimised outputs establish the reference dataset against which both networks are measured; by capturing a broad spectrum of structural responses driven by variations in span, purlin spacing, chord dimensions and load intensity, the dataset provides a suitable baseline for training and validating the MLP and MNM.

The output variables are strongly unequal in difficulty. The riser, vertical chord and column each take only three distinct catalogue values across the whole dataset and the inclined chord four, whereas the rafter steps through eighteen values spanning 1.78 to 18.50 cm². This asymmetry proves to dominate the error statistics of both models.

4.2 Training behaviour

Both networks converged smoothly (Fig. 7). The training and validation curves remain closely aligned throughout, and the validation error decreases monotonically rather than turning upward, indicating that neither network overfits at ten hidden neurons. The MLP continued to improve slowly and reached the 1000-epoch ceiling with its best validation performance at epoch 997; the MNM converged faster in the early epochs and was stopped by the early-stopping criterion at epoch 398, with its best validation performance at epoch 392. Training either network takes a few tens of seconds on a desktop computer, after which a prediction for a new configuration is effectively instantaneous.

International Journal of Engineering Research & Technology (IJERT)
ISSN: 2278-0181
Vol. 15 Issue 08 , August - 2026

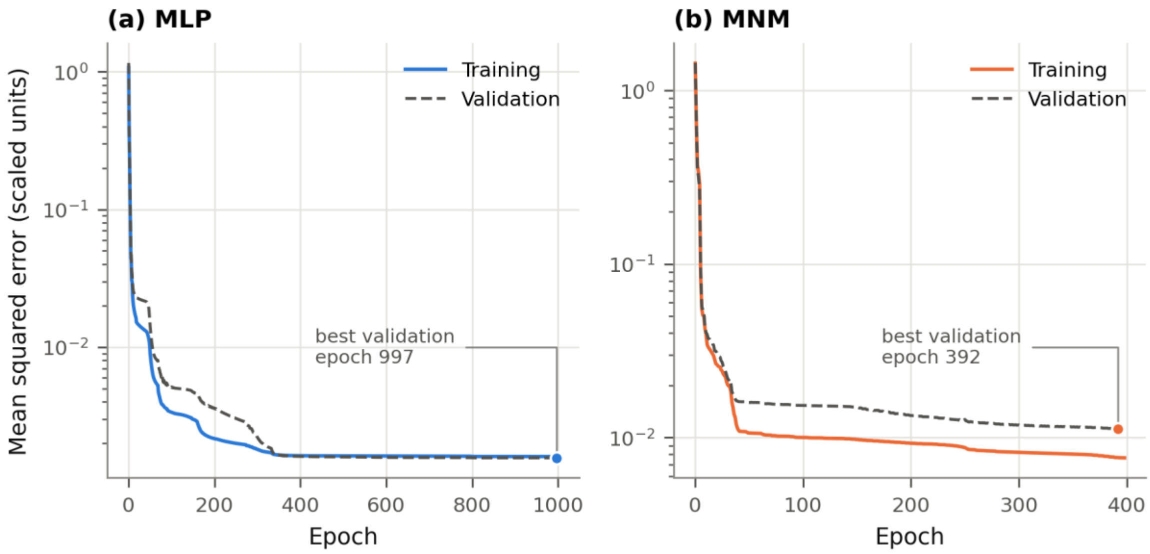

Fig. 7: Performance curves of the networks created. Mean squared error against epoch for (a) the MLP and (b) the MNM, in scaled units.

4.3 Predictive performance under the record-wise partition

With the 384 records divided at random into 269 training, 58 validation and 57 testing configurations, both models reproduce the STAAD.Pro sections closely (Table 5). The MLP achieves an overall RMSE of 0.286 cm² with R = 0.9957 and R^2 = 0.9914; the MNM achieves 0.331 cm² with R = 0.9942 and R^2 = 0.9885. In both cases the training, validation and testing statistics are almost identical, which again indicates that neither model overfits.

Table 5: Predictive performance of the MLP and MNM under the record-wise partition

Model	Split	RMSE (cm²)	MAE (cm²)	MAPE (%)	R	R²
MLP	Training	0.287	0.099	1.56	0.9957	0.9914
MLP	Validation	0.289	0.100	1.63	0.9952	0.9904
MLP	Testing	0.282	0.094	1.58	0.9962	0.9923
MLP	Overall	0.286	0.098	1.57	0.9957	0.9914
MNM	Training	0.330	0.160	2.51	0.9943	0.9886
MNM	Validation	0.343	0.177	2.99	0.9932	0.9864
MNM	Testing	0.323	0.169	2.90	0.9950	0.9900
MNM	Overall	0.331	0.164	2.64	0.9942	0.9885

The regression plots (Fig. 8) show predicted areas clustering tightly about the line of equality for both models, with least-squares fits of Y = 0.992T + 0.049 for the MLP and Y = 0.989T + 0.062 for the MNM slopes within 1.1 % of unity and negligible intercepts, indicating no systematic bias towards over- or under-sizing.

International Journal of Engineering Research & Technology (IJERT)
ISSN: 2278-0181
Vol. 15 Issue 08 , August - 2026

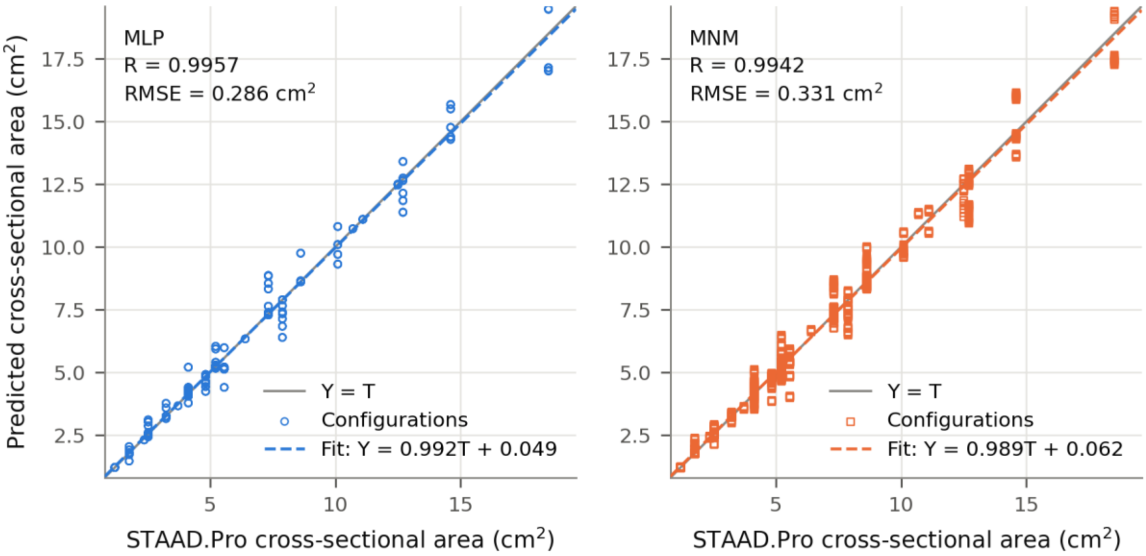

Fig. 8: Regression of predicted against STAAD.Pro cross-sectional areas, all six members pooled, for (a) the MLP and (b) the MNM.

Table 6 reports a worked example for a single configuration a 10 m × 5 m polyhouse with 2 m purlin spacing showing the level of agreement obtained for an individual design.

Table 6: Cross-sectional areas obtained from STAAD.Pro and predicted by the two models for one configuration (length 10 m, span 5 m, purlin spacing 2 m)

Source	Riser	Rafter	Vertical chord	Inclined chord	Purlins	Column
STAAD.Pro (cm²)	5.23	1.78	4.83	4.83	1.21	8.62
MLP (cm²)	5.230	1.748	4.831	4.848	1.208	8.620
MNM (cm²)	5.256	1.770	4.815	4.828	1.203	8.622
Error, MLP − STAAD	0.000	−0.032	+0.001	+0.018	−0.002	0.000
Error, MNM − STAAD	+0.026	−0.010	−0.015	−0.002	−0.007	+0.002

4.4 Member-wise accuracy

Pooled statistics conceal a strong asymmetry between members (Table 7). The MLP is essentially exact for five of the six members: RMSE below 0.01 cm² and a 100 % standard-section hit rate for the riser, vertical chord, purlins and column, and 0.084 cm² for the inclined chord. Almost the entire error budget of both models comes from the rafter, whose eighteen catalogue values and wide range make it by far the hardest target. The MNM is slightly less accurate than the MLP on every member under this partition, with its largest deficits on the column and the riser.

Table 7: Member-wise accuracy under the record-wise partition

Member	MLP RMSE (cm²)	MLP R^2	MLP section hit rate	MNM RMSE (cm²)	MNM R^2	MNM section hit rate
Riser	0.002	1.0000	100.0 %	0.165	0.9767	99.7 %
Rafter	0.696	0.9770	53.4 %	0.739	0.9741	50.8 %
Vertical chord	0.001	1.0000	100.0 %	0.058	0.9447	99.7 %
Inclined chord	0.084	0.9943	100.0 %	0.187	0.9714	90.4 %
Purlins	0.003	1.0000	100.0 %	0.013	0.9997	100.0 %
Column	0.005	1.0000	100.0 %	0.213	0.9560	98.7 %

The error histograms (Fig. 9) are sharply peaked at zero for both models and free of systematic skew. For the MLP, 88.5 % of the 2304 individual member predictions fall within ±0.25 cm² of the STAAD.Pro value; for the MNM the figure is 82.6 %. The residual tails in both cases belong almost entirely to the rafter.

International Journal of Engineering Research & Technology (IJERT)
ISSN: 2278-0181
Vol. 15 Issue 08 , August - 2026

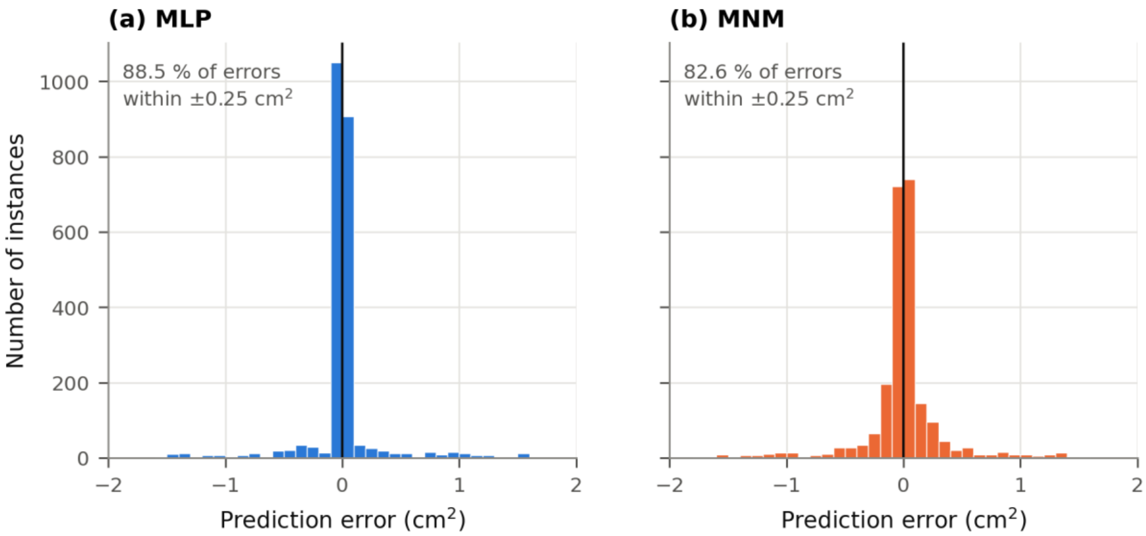

Fig. 9: Error histograms for (a) the MLP and (b) the MNM, all members pooled.

4.5 Generalisation to unseen design cases

As established in Section 3.1, the 384 records comprise 64 design cases repeated at six polyhouse lengths, and length does not affect any output. Under the record-wise partition of Section 4.3, every testing record therefore has five identical-target twins inside the training set, and the testing error measures recall rather than generalisation. To separate the two, both models were retrained with entire design cases withheld: 45 cases for training, 10 for validation and 9 for testing, corresponding to 270, 60 and 54 records. All other settings were unchanged.

The results are given in Table 8. Testing RMSE rises from 0.282 to 0.402 cm² for the MLP and from 0.323 to 0.453 cm² for the MNM, and the proportion of configurations for which all six standard sections are chosen correctly falls from 53.4 % to 35.9 % (MLP) and from 48.7 % to 32.0 % (MNM). Both models nevertheless retain R^2 above 0.97 and MAPE below 5.1 % on geometries they have never seen, which supports their use as preliminary-design surrogates; but it is this second set of figures, not the first, that should be quoted as generalisation performance.

Table 8: Predictive performance with entire design cases withheld

Model	Split	RMSE (cm²)	MAE (cm²)	MAPE (%)	R^2
MLP	Training	0.398	0.223	3.87	0.9841
MLP	Validation	0.503	0.293	5.22	0.9724
MLP	Testing	0.402	0.243	4.32	0.9796
MNM	Training	0.372	0.194	3.64	0.9861
MNM	Validation	0.656	0.340	5.92	0.9530
MNM	Testing	0.453	0.251	5.09	0.9741

The member-wise picture changes materially under this harder test (Fig. 10). The MLP loses its near-exact accuracy on the members it previously reproduced perfectly the vertical chord rises from 0.001 to 0.107 cm², the column from 0.005 to 0.350 cm² because those predictions were, in effect, retrievals. Under the grouped partition the MNM is the more accurate model on four of the six members: vertical chord (0.067 against 0.107 cm²), inclined chord (0.233 against 0.406 cm²), column (0.249 against 0.350 cm²) and, marginally, the riser. The MLP retains a clear advantage only on the rafter (0.803 against 0.971 cm²), which is sufficient to give it the better pooled statistic.

International Journal of Engineering Research & Technology (IJERT)
ISSN: 2278-0181
Vol. 15 Issue 08 , August - 2026

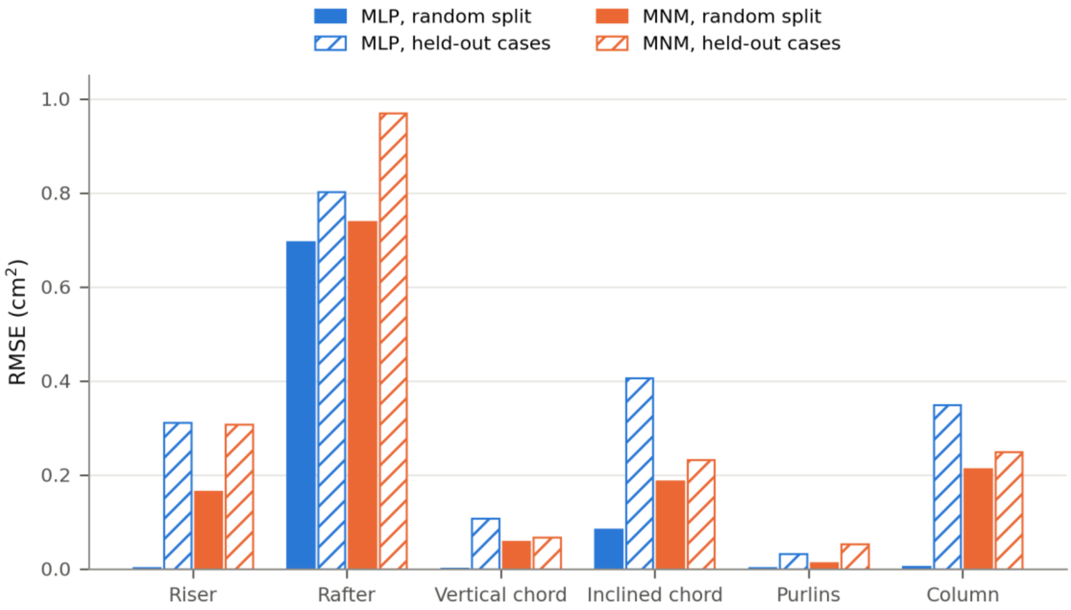

Fig. 10: Member-wise RMSE under the two partitioning schemes. Solid bars: random record-wise partition. Hatched bars: entire design cases withheld.

4.6 Effect of network size

Refitted at the hidden-layer size selected by the parametric sweep and under the record-wise partition, the MLP with 19 hidden neurons reproduces the design table with an overall RMSE of 5×10^{-6} cm² the largest single deviation across all 2304 member predictions being 6×10^{-5} cm² and selects the correct standard section for all six members in 100 % of configurations. The MNM with 18 hidden neurons reaches an overall RMSE of 0.109 cm² ($R^2 = 0.9988$) with a 75.0 % all-six section hit rate, its remaining error again concentrated in the rafter (0.264 cm²). These figures should be read alongside Section 4.5: a network large enough to interpolate the 64-case design table exactly does so, but that does not by itself demonstrate an ability to size a truss geometry outside the table.

4.7 Comparison of the MLP and the MNM

Under the record-wise partition the MLP is the more accurate model at every hidden-layer size beyond six neurons, and decisively so once the network is large enough to fit the design table exactly. Under the grouped partition the ranking is no longer uniform: the MLP holds a modest overall advantage that comes entirely from the rafter, while the MNM predicts four of the six members more accurately.

This is the pattern the multiplicative formulation would be expected to produce. Members whose sizing is governed smoothly by a product of span and load intensity the vertical chord, the inclined chord and the column are handled better by neurons that form such a product directly. The rafter, which steps through eighteen catalogue sizes and therefore demands a sharp, piecewise response, favours the additive network, whose tansig units can be combined into steep local transitions more readily than a product of eight affine terms can. The MNM also achieves its accuracy with a network that converged in 398 epochs against the MLP's 1000, though it carries more free parameters at the same hidden-layer width (226 against 156).

For practical purposes the MLP is the better single surrogate for this dataset, and the MNM is a competitive alternative for the geometry-governed members. A composite predictor the MLP for the rafter and the MNM for the remaining members would outperform either model alone on the held-out design cases, and is a natural direction for further work.

4.8 Economy of section type

In addition to evaluating predictive performance, the study investigated the economic suitability of different steel section types for polyhouse roof trusses. Comparative analyses performed in STAAD.Pro indicated that Circular Hollow Sections provide the most economical and structurally efficient solution owing to their favourable strength-to-weight ratio, lower material consumption, ease of fabrication, reduced self-weight and simplified installation. Although I-sections and T-sections possess higher load-carrying capacities, their increased material requirements and fabrication complexity make them less suitable for lightweight polyhouse structures, while channel sections offer only moderate economic benefits. The close agreement between the MLP and MNM predictions and the STAAD.Pro design results demonstrates that the optimum selection of CHS members can be reliably obtained from a trained network, reducing dependence on repetitive finite element analyses without compromising structural safety or design accuracy.

4.9 Limitations

Three limitations should be borne in mind when interpreting these results. First, the dataset resolves to 64 independent design cases rather than 384; polyhouse length is present as an input but exerts no influence on the targets, and the remaining six inputs are determined by width and purlin spacing. The effective input dimensionality is therefore two, and the accuracy reported in Section 4.5 rather than Section 4.3 should be regarded as the generalisation figure. Extending the dataset so that length, panel-point distribution and the three load components vary independently would

International Journal of Engineering Research & Technology (IJERT)
ISSN: 2278-0181
Vol. 15 Issue 08 , August - 2026

both strengthen the models and allow the full eight-input formulation to be exercised.

Second, all predictions are interpolations within the ranges listed in Table 2. Applying either network outside those ranges spans wider than 20 m, wind loads above 19.1 kN/m² is extrapolation and should be verified against a STAAD.Pro run.

Third, the networks predict a continuous area, while design requires a discrete catalogue section. Rounding to the nearest available section, as reported through the hit rate, is a practical remedy, but a network trained directly as a classifier over the catalogue sections would align the objective with the design decision and is likely to raise the rafter accuracy that currently limits both models.

CONCLUSION

This study demonstrates the effectiveness of the Multilayer Perceptron and the Multiplicative Neuron Model for predicting the optimum cross-sectional areas of steel pipe members in Howe-type polyhouse roof trusses. A dataset of 384 STAAD.Pro-generated truss configurations enabled both models to learn the relationships between geometric parameters, loading conditions and member requirements, and training both architectures with an identical Levenberg–Marquardt procedure on identical data isolated the effect of the neuron model itself.

Under a conventional random partition, the MLP achieved an overall RMSE of 0.286 cm² with R = 0.9957 and the MNM 0.331 cm² with R = 0.9942, closely reproducing the results of detailed finite element analysis. Because the dataset comprises 64 design cases repeated at six polyhouse lengths, both models were also evaluated with entire design cases withheld; testing RMSE then became 0.402 cm² for the MLP and 0.453 cm² for the MNM, with R^2 above 0.97 in both cases. The MLP was the more accurate model overall, but the advantage came entirely from the rafter: on the vertical chord, inclined chord and column the MNM predicted more accurately, consistent with its capacity to represent products of span and load within a single neuron.

Both models predict the six member sizes in a fraction of a second, against a full analysis-and-design cycle per configuration in STAAD.Pro, enabling rapid assessment of design alternatives and supporting preliminary design, parametric study and structural optimisation. The study further establishes Circular Hollow Sections as the most suitable members for polyhouse roof trusses on grounds of strength-to-weight ratio, material efficiency, ease of fabrication and cost.

Overall, the proposed MLP–MNM framework provides a reliable and computationally efficient surrogate modelling approach for polyhouse roof truss design. Extending the dataset so that length and the load components vary independently, and reformulating the task as classification over standard catalogue sections, are the two developments most likely to improve on the accuracy reported here.

REFERENCES

[1] Amir, H. M., & Hasegawa, T. 1988. Greenhouse structure design optimization. J. Irrig. Eng. Rural Plan, (14): 33–52.

[2] Choi, Yun, and Yoon. 2014. Survey analysis of the characteristics of greenhouses in Korea. Int. J. Environ. Rural Dev., 5(1).

[3] Farooq, F., Amin, N. M., Khan, K., Sadiq, R. M., Javed, M. F., Aslam, F., & Alyousef, R. 2020. A comparative study of random forest and genetic engineering programming for the prediction of compressive strength of high strength concrete (HSC). Appl. Sci., 10(20): 1–18.

[4] Gao, Y., & Yang, X. 2021. Research on deep convolutional neural network in damage identification of truss structure. In: IOP Conference Series: Earth and Environmental Science (LIMIT-2021), pp. 12–33.

[5] Ghani, S., Bakochristou, F., ElBialy, E. M. A. A., Gamaledin, S. M. A., Rashwan, M. M., Abdelhalim, A. M., & Ismail, S. M. 2019. Design challenges of agricultural greenhouses in hot and arid environments: a review. EAEF, 12(1): 48–70.

[6] Gupta, D., Santosh, D. T., Debnath, S., Maitra, S., & Gaikwad, D. 2020. Modeling and simulation application for greenhouse microclimatic studies and structural analysis. PCSA, 300–312.

[7] Hagan, M. T., & Menhaj, M. B. 1994. Training feedforward networks with the Marquardt algorithm. IEEE Trans. Neural Netw., 5(6): 989–993.

[8] IS 800. 2007. General construction in steel-code of practice. Bureau of Indian Standards, New Delhi, India.

[9] IS 875, Part 1. 2015. Code of practice for design loads (other than earthquake) for buildings and structures-dead loads. Bureau of Indian Standards, New Delhi, India.

[10] IS 875, Part 2. 2015. Code of practice for design loads (other than earthquake) for buildings and structures-imposed loads. Bureau of Indian Standards, New Delhi, India.

[11] IS 875, Part 3. 2015. Code of practice for design loads (other than earthquake) for buildings and structures-wind loads. Bureau of Indian Standards, New Delhi, India.

[12] IS 1161. 2014. Steel tubes for structural purposes-specification. Bureau of Indian Standards, New Delhi, India.

[13] IS 14462. 1997. Recommendations for layout, design and construction of greenhouse structures. Bureau of Indian Standards, New Delhi, India.

[14] Kalyanshetti, M. G., & Mirajkar, G. S. 2012. Comparison between conventional steel structures and tubular steel structures. Int. J. Eng. Res. Appl., 2(6): 1460–1464.

[15] Kendirli, B. 2006. Structural analysis of greenhouses: a case study in Turkey. Build. Environ., 41(7): 864–871.

[16] Krishna, D. A., Priyadarsini, R. S., & Narayanan, S. 2021. High temperature effects on different grades of concrete. Sadhana, 46(1): 1–12.

[17] Liu, Z., Jiang, A., Shao, W., Zhang, A., & Du, X. 2021. Artificial-neural-network-based mechanical simulation prediction method for wheel-spoke cable truss construction. Int. J. Steel Struct., 21(3): 1032–1052.

[18] Mehrjoo, M., Khaji, N., Moharrami, H., & Bahreininejad, A. 2008. Damage detection of truss bridge joints using artificial neural networks. Expert Syst. Appl., 35(3): 1122–1131.

[19] Nguyen, D., & Widrow, B. 1990. Improving the learning speed of two-layer neural networks by choosing initial values of the adaptive weights. In: Proceedings of the International Joint Conference on Neural Networks, San Diego, 3: 21–26.

[20] Patrikar, A., & Pathak, K. K. 2016. Fully stressed design of Fink truss using STAAD.Pro software. Open J. Civ. Eng., 6(4): 631–642.

[21] Saltuk, B. 2019. Structural analysis example of steel construction greenhouses. ABTD, (16): 61–68.

[22] Satpaise, W. B., & Lande, S. P. 2005. Optimization of different types of steel trusses using fully stressed design concept. IETIR, (1): 1–17.

[23] Saxena, S., & Pathak, K. K. 2015. Application of artificial neural networks for fully stressed design of Pratt and Howe truss. New Technologies Sci. Eng., (2): 94–103.

[24] Singh, L., Kaushal, A., & Digra, A. 2021. A review on stability of polyhouse structures. Int. J. Agric. Sci., 17: 285–291.

[25] Yadav, R. N., Kalra, P. K., & John, J. 2007. Time series prediction with single multiplicative neuron model. Appl. Soft Comput., 7: 1157–1163.